Eigenstate-resolved unimolecular dissociation dynamics of HOCl at $v_{OH} = 7$ and 8

Andrea Callegari, Roman Schmied, Patrice Theulé, Julia Rebstein and Thomas R. Rizzo*

Laboratoire de chimie physique moléculaire (LCPM), Ecole Polytechnique Fédérale de Lausanne, CH-1015 Lausanne, Switzerland. E-mail: thomas.rizzo@epfl.ch

We use infrared–visible double-resonance overtone excitation to prepare HOCl molecules in single, well-characterized rotational levels of the high OH stretching states $v_{OH} = 7$ and $v_{OH} = 8$. This work extends our recent studies on HOCl dissociation dynamics to higher energies above the dissociation threshold on the ground potential energy surface. In spite of a rapid increase of the vibrational coupling with v_{OH}, unimolecular dissociation is still limited by the rate at which energy initially deposited in the OH stretch leaks out into the reaction coordinate. We observe that the increased coupling is not sufficient to put the molecule in the statistical limit, even at the energy of $v_{OH} = 8$, which is 5000 cm^{-1} above the dissociation threshold. This implies that a microcanonical ensemble of HOCl molecules prepared even at an energy substantially higher than the dissociation threshold should exhibit non-exponential decay, contrary to the assumptions of statistical theories.

I. Introduction

While the notion that unimolecular dissociation is intimately related to vibrational energy redistribution dates back almost three quarters of a century,[1–3] the ability to observe directly the connection between these two phenomena has only recently become possible. If intramolecular vibrational energy redistribution (IVR) is fast and complete on the timescale of chemical bond breaking, the dissociation rate of molecules in individual states usually falls within a narrow interval around the average rate, which can be calculated to a sufficient accuracy by statistical theories.[4,5] While unimolecular reaction studies performed in a non-state-resolved manner reveal dissociation rates that appear to be in good agreement with the predictions of such theories, the distribution of reactant energies prevents one from directly establishing the relative timescales of IVR and unimolecular dissociation. In the case that IVR is slow and/or incomplete on the timescale of chemical bond breaking, different states can have widely different dissociation rates, depending on how well their vibrational energy couples to the reaction coordinate. It is only in the last 15 years that advances in experimental techniques have allowed the study of unimolecular dissociation at the fully state-resolved level, which is necessary to observe these widely varying rates. Such studies provide the most stringent test of unimolecular reaction theories, since the loss of information caused by averaging over the ensemble of initially prepared molecules is eliminated.

A variety of techniques have been used to investigate unimolecular reactions at the state-resolved level with the goal of determining the limits of statistical assumptions:[6–18] linewidth analysis of transitions to quasi-bound states of H_2CO, D_2CO, HCO; spectroscopic probing of the disappearance of the excited reactant from single states of HFCO and CH_3O prepared by SEP; and spectroscopic detection of the dissociation fragments of selectively excited CH_2CO, HN_3 and HOOH. Recently, both our group[19–21] and that of Sinha[22–24] have investigated the unimolecular dissociation dynamics of HOCl from highly-excited vibrational states prepared by double-resonance vibrational overtone excitation. These studies demonstrate that dissociation rates are slow and limited by IVR when the molecule is initially prepared with 6 quanta in the OH stretching mode. We attributed this to weak coupling between the initially prepared state and the bath of all other vibrational states, particularly those highly excited in the dissociation coordinate. However, studies such as these over a small range of vibrational energy leave important questions about the intramolecular dissociation dynamics unanswered: Is the IVR-limited dissociation rate a general property of states prepared with all the excitation in the OH stretch, or is it specific to the (6,0,0) state, which is just above the dissociation threshold? If it does persist at higher energy, where does the transition to statistical behavior occur? In order to answer these questions and further test our modeling of the dissociation dynamics, we have undertaken an investigation of HOCl excited to the (7,0,0) and (8,0,0) levels. The results and ideas presented here build on previous experimental and theoretical work on HOCl spectroscopy, potential energy surface and dynamics.[19–56]

Given the tight connection with our previous work, analysis of the current results is based in a straightforward way on the models and concepts presented therein. In particular, we employ the same notation as in papers I and II of this series.[20,21] When referring to vibrational states of HOCl, we use the notation (n_1, n_2, n_3) to indicate the number of quanta in the OH stretching, HOCl bending and OCl stretching modes respectively. These states are zeroth-order states—that is they are not eigenstates of the full Hamiltonian, but only of an approximate Hamiltonian that is separable in the above-mentioned coordinates. We use J, K_a and K_c to label rotational states, although since HOCl is nearly a symmetric top, simply J and $K(= K_a)$ are often sufficient.

II. Experimental approach

The experimental approach for the work presented here is similar to that described in our recent report on the eigenstate-resolved spectroscopy of HOCl in the region of (6,0,0),[20,21] and only the relevant changes are discussed in

detail here. Briefly, an infrared laser pulse promotes HOCl molecules in a static gas cell to a specified rovibrational state of the (2,0,0) level. Approximately 20 ns later, a second pulse from a visible dye laser promotes the pre-selected molecules to single rovibrational states of the desired vibrational state, (7,0,0) or (8,0,0), which lie above the threshold for dissociation into HO + Cl. The resulting OH fragments are then probed by laser-induced fluorescence (LIF) *via* the A–X band. In a typical experiment, the frequencies of the IR state-selection laser and of the UV probe laser are set, respectively, to prepare a HOCl reactant molecule in the desired rotational state of (2,0,0) and to detect OH products in a convenient state. The frequency of the overtone dissociation laser is then scanned over the region of interest for each intermediate state, producing a photofragment excitation spectrum.

While this scheme works well for investigating the (6,0,0) and (7,0,0) regions, several factors conspire to render signal-to-noise ratio unsatisfactory for excitation to (8,0,0). First, the oscillator strength of the vibrational transitions from the intermediate state decreases roughly exponentially with the difference of vibrational quanta between the initial and final state. Moreover, the amount of energy deposited in the fragments upon dissociation increases with the energy of the initially prepared reactant state, populating a broader distribution of product states. Since we probe only one product state at a time, most of the dissociation fragments inevitably escape detection. Thus, the broader product state distribution at higher energy leads to reduced detection sensitivity. Finally, broadening of the linewidths, as discussed in Section III.B, further decreases the transition probability, since the oscillator strength is distributed over a larger frequency range. To compensate for this loss of sensitivity, we employ a double resonance scheme that uses the (4,0,0) level as the intermediate vibrational state. Compared to the previous scheme, the 300-fold smaller oscillator strength of this first transition[40] is partially compensated by the 10-fold increase in available laser power in the corresponding frequency region. Moreover, the transition strength for the second transition is larger, and the available laser power remains roughly the same, thus giving a significantly better signal-to-noise ratio for the $4\nu_1 \leftarrow 0$, $8\nu_1 \leftarrow 4\nu_1$ double-resonance scheme.

The laser pulses for the various excitation steps are generated as follows. For pumping the $2\nu_1 \leftarrow 0$ transition, we mix the output of a Nd:YAG pumped dye laser with the single mode output of the YAG in a LiNbO$_3$ crystal to produce 2–4 mJ infrared pulses in the range 6600 to 7300 cm^{-1}. For the $4\nu_1 \leftarrow 0$ transition, we operate the dye laser on LDS751 to produce 50 mJ of visible radiation, which is used without further mixing. Operating the laser with an intra-cavity etalon narrows the linewidth to 0.02 cm^{-1}, and this value is largely preserved after mixing. For dissociating the state-selected molecules, a second dye laser, operating on LDS698 ($7\nu_1 \leftarrow 2\nu_1$), Rh610 + Rh590 ($8\nu_1 \leftarrow 2\nu_1$), or LDS925 ($8\nu_1 \leftarrow 4\nu_1$), provides pulse energies of 50 mJ within a linewidth of 0.15 cm^{-1}. When required, we reduce this to 0.02 cm^{-1} by inserting an intra-cavity etalon. Finally, for LIF detection of the resulting OH fragments, we use the frequency-doubled output of a Nd:YAG pumped dye laser, operating with Rhodamine 640.

We prepare HOCl *in situ* by flowing H$_2$O and Cl$_2$ at a pressure of several mTorr in a glass column packed with glass beads and yellow HgO. The resulting products flow continuously through a glass fluorescence cell at a typical working pressure of 20–50 mTorr.

III. Results

A. Overview and spectroscopic analysis

Fig. 1 and 2 show stacks of typical double-resonance spectra obtained for the $7\nu_1 \leftarrow 2\nu_1$, $8\nu_1 \leftarrow 4\nu_1$ bands, respectively. For each spectrum in the stack, we fix the state-selection laser frequency to prepare HOCl molecules in a single rovibrational level characterized by rotational numbers J' and K' as indicated in the figure. We then scan the frequency of the overtone excitation laser over the region of interest while collecting the total OH fluorescence induced by the probe laser. In spite of an obvious similarity in overall appearance, the two regions investigated show important differences. We discuss the general spectroscopic analysis first, and then separately discuss the specific features of each spectral region.

In order to assign the main transitions in each spectrum, we use our knowledge of the rotational assignment of the intermediate state together with the relevant selection rules. Additional features could originate from either splitting of the main transitions by vibrational coupling of the bright state to dark states, or to incomplete state selection in the first step. Being able to distinguish these two cases is of critical importance, as vibrational coupling reflects the IVR dynamics of the initially prepared state while incomplete state selection is simply an artifact of our experimental procedure. The use of combination differences, in which we compare spectra that terminate on the same final state from different intermediate states, allows us to classify these additional features and decide accordingly whether or not to include them in our analysis.

Further information about vibrational coupling comes from quantitative analysis of the line positions using a standard vibration–rotation Hamiltonian. As discussed in papers I and II in this series, this approach provides sensitive information about presence of perturbations (*i.e.*, vibrational coupling), which in turn allows us to interpret the dynamics. Observing deviations of the energy levels from their expected position provides the means to detect couplings between vibrational levels that may be too weak to result in additional spectral features. Moreover, the molecular constants obtained from the fit (band origin, rotational constants, *etc.*) help characterize the identity of the observed vibrational states. Specifically, we fit the spectra to Watson's *s*-reduction Hamiltonian including terms up to fourth order:[57,58]

$$H = H_0 + \bar{B}J^2 + (A - \bar{B})J_z^2 + \Delta(J_+^2 + J_-^2) - (D_J)(J^2)^2$$
$$- (D_{JK})J^2J_z^2 - (D_K)(J_z^2)^2$$

$$\bar{B} = \frac{B + C}{2}$$

$$\Delta = \frac{B - C}{4} \tag{1}$$

Comparison with the molecular constants of previously measured lower OH stretching overtones helps us further characterize the nature of the initially prepared state.

1. The (7,0,0) region. Each spectrum displayed in Fig. 1 is characterized by two prominent spectral features accompanied by a few weaker ones. The identity of these transitions is readily determined: the strong transitions correspond to P and R branches of a parallel ($\Delta K_a = 0$) band, and the weaker ones to the perpendicular ($\Delta K_a = \pm 1$) component. It is interesting to note the large intensity ratio ($>10:1$) between the parallel and perpendicular components of the transition. According to the selection rules, this corresponds to a transition dipole moment oriented mostly along the *a*-axis, which corresponds approximately to the O–Cl bond. This finding is far from unexpected, in spite of the fact that a bond-dipole model would predict a band that was polarized almost entirely perpendicular to the O–Cl bond. The experimentally observed trend for lower overtones of HOCl,[20,28–30,36] as well as for HOD,[59] HOOH[18] and CH$_3$OH[60] shows the parallel component increasing with the number of OH vibrational stretch quanta. It is clear that pulling the H atom away to infinity would change the electronic distribution of the
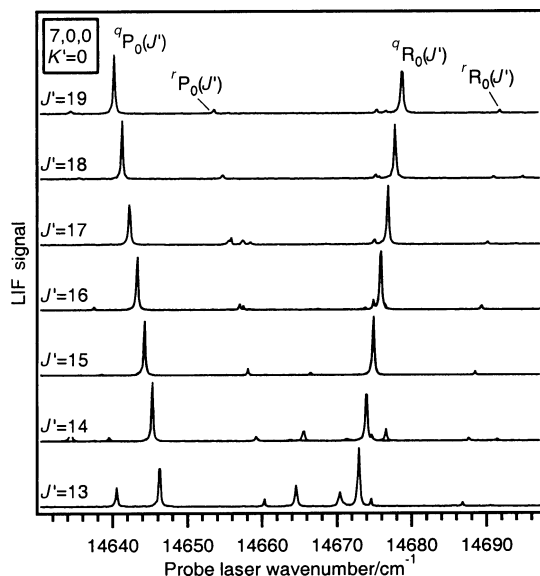
Fig. 1 Representative double-resonance spectra of the $7\nu_1 \leftarrow 2\nu_1$ band of HOCl.

that unlike the spectra in the (6,0,0) region, the (7,0,0) spectra show no obvious sign of splitting due to vibrational coupling. Further evidence pointing in this direction comes from quantitative analysis of the spectra with the asymmetric rotor Hamiltonian of eqn. (1). As is shown in Table 1, the data set available for (7,0,0) allows determining all molecular constants in eqn. (1) to good accuracy. No sign of perturbation is evident from the residuals of the fit—out of 152 measurements corresponding to about 30 different rotational states, only two deviate more than 0.1 cm^{-1} from their calculated value. For the remaining measurements, the rms deviation amounts to 2.4×10^{-2} and 0.8×10^{-2} cm^{-1} respectively for line positions extracted from medium resolution (0.15 cm^{-1}) spectra and high resolution (0.02 cm^{-1}) scans of individual lines. In paper I we discussed how, in the (6,0,0) region, patterns of deviation in the residuals of the fit reveal the presence of perturbing states.[20] These dark perturbing states have different

Table 1 Molecular constants (cm^{-1}) of HO ^{35}Cl for the (7,0,0) and (8,0,0) states. Uncertainty in the last digit corresponding to one standard deviation is given in parentheses

	(7,0,0)	(8,0,0)
E	21 709.2166(36)	24 101.89
$A - \bar{B}$	14.730 49(272)	13.92
$\bar{B}$	0.495 551 1(148)	0.4945
$B - C$	0.016 585(38)	0.025
$D_J \times 10^6$	0.4861(267)	2.0
$D_{JK} \times 10^4$	0.611(58)	0.4065^a
$D_K \times 10^2$	1.190(61)	0.4333^a

^{a} Fixed to ground state value.

resulting free radical along the remaining bond coordinates, which in the case of HOCl would be the O–Cl bond. Thus, for a finite OH bond elongation, one can expect the dipole moment to change along the O–Cl bond axis.
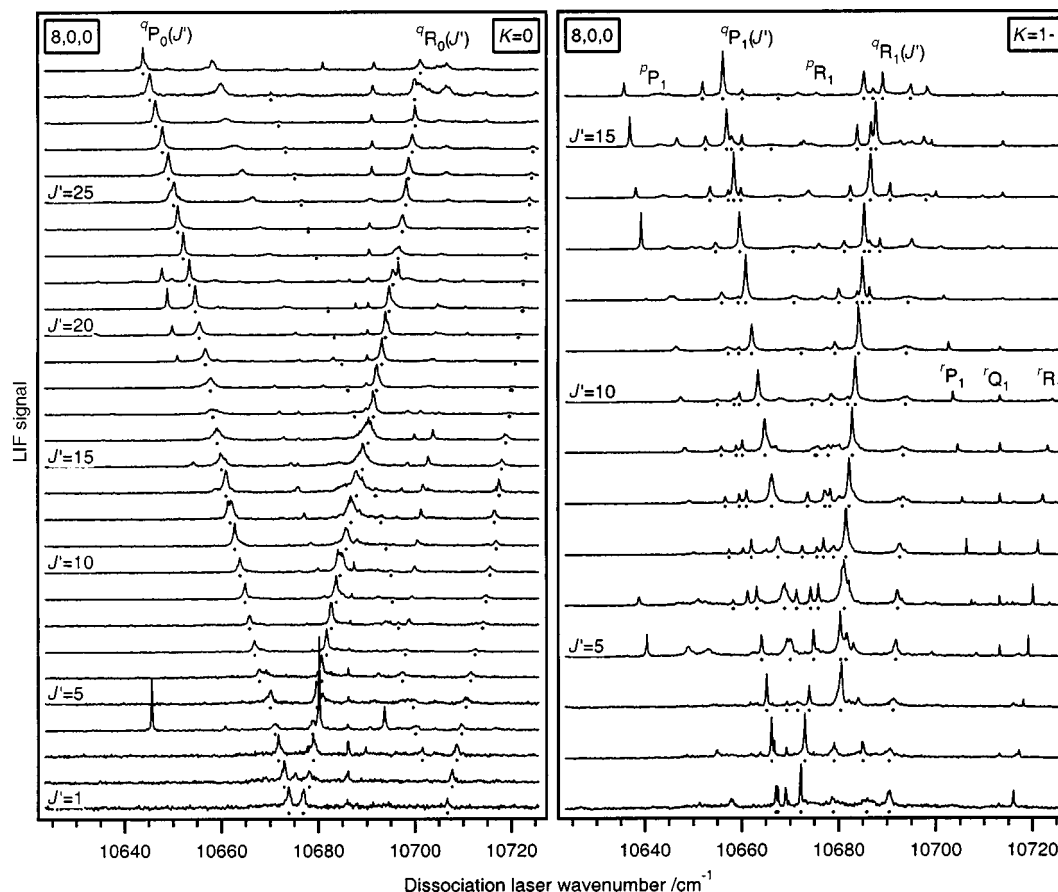
A few spectra, most notably those at $K = 0$, show additional features that are readily identified by combination differences as spurious transitions arising from incomplete state-selection. Once these are eliminated, it becomes clear
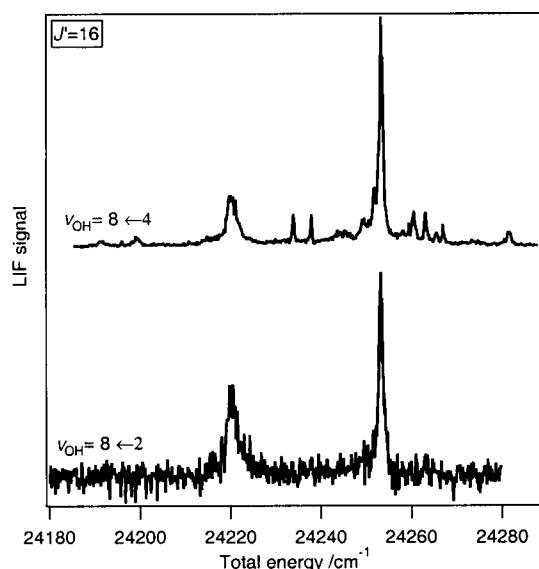

Fig. 2 Double-resonance spectra of the $8\nu_1 \leftarrow 4\nu_1$ band of HOCl. Left panel: $K = 0$; right panel: $K = 1$, lower asymmetry splitting component. Peaks marked with a dot belong to the ^qP and ^qR parallel branches and reflect vibrational coupling between the bright state and dark bath states. Unmarked peaks arise from the weaker perpendicular transitions or from incomplete selection in the intermediate step and do not reflect vibrational coupling, as explained in the text.

rotational constants than the bright state, hence they tune in and out of resonance at different rotational quantum numbers. The lack of this kind of perturbation does not imply that (7,0,0) is not mixed with other vibrational states. If this were the case, molecules promoted to this level would not dissociate. The correct interpretation is that within our detection limits, vibrational mixing is uniform across the range of rotational states probed in the experiment. In other words, none of the states that come into resonance with the bright state is sufficiently strongly coupled to it to produce a detectable displacement from its expected position.

On the other hand, non-resonant coupling (*i.e.* coupling with states that remain far in energy across the whole range of rotational states investigated) can often be detected through unphysically large distortion constants, even if the perturbing state is not visible in the spectrum. These account for the high order terms in the rotational energy dependence of a state arising from interaction with a perturbing state with a different set of rotational constants. In this particular case, the value of $D_k = 1.19 \times 10^{-2}$ obtained from the fit is almost three times larger than the ground state value, while the extrapolation from lower overtones[20,28–30] would predict a 28% decrease. This strongly suggests the presence of such non-resonant coupling.

2. The (8,0,0) region. Comparison between the spectra in the (7,0,0) (Fig. 1) and (8,0,0) (Fig. 2) regions reveals a number of extra peaks in the latter. Combination differences confirm that most of these peaks arise from splitting of the zeroth-order bright state and not from incomplete state selection. As shown in Fig. 3, we further verify this assessment by comparing the two sets of spectra that access the (8,0,0) level *via* different intermediate vibrational states (*i.e.*, the $8\nu_1 \leftarrow 4\nu_1$ and $8\nu_1 \leftarrow 2\nu_1$ bands). The strong similarity of the additional spectral features (*i.e.*, line positions and width) indicates that they reflect splittings of the (8,0,0) level. The poor agreement obtained from a fit of the (8,0,0) spectra with the asymmetric rotor Hamiltonian of eqn. (1), with discrepancies of the order of a few cm^{-1}, reinforces this conclusion and confirms the existence of significant coupling between the bright state and certain bath states.

Fig. 3 Comparison between double-resonance spectra of the $8\nu_1 \leftarrow 2\nu_1$ (bottom) and $8\nu_1 \leftarrow 4\nu_1$ (top) band of HOCl. The two spectra reach the same final state (8,0,0) *via* different intermediate vibrational states, (2,0,0) and (4,0,0) respectively, hence, their common spectral features reflect solely the properties of the final state. Notice the better signal-to-noise obtained with the second excitation scheme.

We previously found that the vibrational interaction between the (6,0,0) level and the bath of dark states is weak compared to the average level spacing, and hence at most one bath state at a time perturbs significantly the bright state.[21] In this case the interaction can be modeled by a 2×2 matrix and the perturbing state can be included in the fit. The same treatment applied to the (8,0,0) spectra does not dramatically improve the fit, however. This indicates that the average coupling strength is comparable with the average level spacing, and that quantitative agreement can be obtained only if interaction between all vibrational states is taken into account by diagonalizing the full Hamiltonian. Unfortunately the amount of information provided by the spectra is not sufficient for this task, since we observe only a handful of levels.

B. Linewidths and dissociation rates

The unimolecular dissociation rates of HOCl molecules promoted to the (6,0,0) level are sufficiently slow that we were able to measure them by scanning the time delay between the dissociation and probe laser while monitoring the appearance of OH fragments.[21] The same is not true for dissociation from the (7,0,0) and (8,0,0) levels investigated here, as the unimolecular dissociation processes occurs on a time scale that is too fast to be resolved by the convolution of the two 5–8 ns laser pulses. However, the Lorentzian linewidth, Γ, that arises from the finite lifetime of the initially prepared quasibound state, is sufficiently large compared to our spectral resolution that we can determine it directly from our frequency resolved spectra. This Lorentzian linewidth can be directly related to the unimolecular reaction rate k:

$$k = \Gamma/\hbar \approx 1.88 \times 10^{11}\ \text{s}^{-1}\Gamma/\text{cm}^{-1} \qquad (2)$$

1. Linewidths of transitions to (7,0,0). The (7,0,0) spectra we observed exhibit relatively narrow features, consistent with a previous study of Barnes and Sinha,[23] which cited an upper limit of 0.05 cm^{-1} for the contribution to the linewidth from lifetime broadening. It thus requires special care to separate lifetime broadening from other sources of spectral broadening of comparable magnitude. Apart from pressure broadening, which is negligible on the timescale of the experiment, and Doppler broadening, which is accounted for exactly, there are two other potential sources contributing to the spectral width that must be considered—power broadening and finite laser linewidth. Power broadening arises from saturating the spectral transition, and we control it simply by decreasing the power of the dissociation laser with neutral density filters to a sufficiently low level. In paper I we determined that the contribution of power broadening to the linewidth of the $6\nu_1 \leftarrow 2\nu_1$ transition is negligible at 4 mJ pulse energy.[20] Since the $7\nu_1 \leftarrow 2\nu_1$ band is weaker, power broadening of the linewidths at the same pulse energy will be even less.

We use an intra-cavity etalon to reduce the laser linewidth for these measurements from 0.15 to ~ 0.02 cm^{-1}, which is comparable with the Doppler broadened linewidths. We verify the laser linewidth using a spectrum analyzer, although not simultaneously with our measurements. We take a conservative estimate of ± 0.01 cm^{-1} for the uncertainty of the actual laser width at the time of the experiment. Combined with 0.025 cm^{-1} Doppler broadening, this gives an instrumental linewidth of between 0.027 and 0.039 cm^{-1}. We extract the lifetime broadened linewidth of spectroscopic transitions by fitting their profiles to a Voigt function[61,62] that accounts for Doppler broadening and finite laser linewidth. The dominant source of error in the deconvolution process is the uncertainty of the laser width, hence the results of the deconvolution have the same ± 0.01 cm^{-1} uncertainty.

All of the 15 lines investigated have a Lorentzian width falling in the range 0.015–0.035 cm^{-1}, which is just below the 0.05 cm^{-1} upper limit of Barnes and Sinha and compares well

with the results of recent theoretical calculations by Schinke's group[63] and Bowman's group[55] who report values of 0.025–0.035 and 0.01 cm^{-1} respectively. The dissociation rates corresponding to our measured linewidths fall between 2.8×10^9 and 6.6×10^9 s^{-1}, faster than the average rates observed at (6,0,0), but still three orders of magnitude lower than the average rate calculated with the statistical adiabatic channel model (SACM).[42]

In contrast to the observed behavior at (6,0,0),[21] the measured dissociation rates at (7,0,0) do not exhibit prominent variations with rotational quantum numbers. The rates for dissociation from $K = 1$ and 2 levels fall in a small interval around their average, while those from $K = 0$ levels increase slowly and smoothly with J. As is discussed more fully below, this lack of strong state-to-state rate variations is expected, partly because of the smaller set of rotational states investigated at (7,0,0), and partly because of the larger number of product channels available for dissociation.[8,64]

2. Linewidths of transitions to (8,0,0). The bottom panels of Fig. 4 show the measured widths of transitions to (8,0,0) for the states with $K = 0$ (left) and $K = 2$ (right). Putting one additional vibrational quantum in the OH stretching coordinate increases the width of the transitions by 1–2 orders of magnitude compared to those at (7,0,0), yielding linewidths in the range from 0.2 to 2.5 cm^{-1}, with an average of 0.75 cm^{-1}. Remarkably, the widths do not exhibit the same kind of uniformity observed at (7,0,0); neither do they exhibit the strong state-to-state fluctuations observed at (6,0,0). Rather, at $K = 0$ the plot of linewidth vs. J exhibits several peaks, suggestive of perturbations from individual dark states that tune into and out of resonance. Fig. 4 confirms this notion by showing together the J dependences of reduced energies (top panels) and widths (bottom panels) of the states investigated. This figure clearly demonstrates a correspondence between the patterns in the top and bottom panels, although the presence of several perturbing states makes this correspondence less intu-

itive than in the simple case of interaction with a single perturbing state. A peak in the bottom panel corresponds to a sudden displacement of the reduced energy from a smooth line in the upper panel, as would be expected for such a perturbation. The left side of Fig. 4 shows that a similar pattern is there for $K = 2$, and in this case the number of perturbing states and the strength of their coupling is smaller, thus leading to an even clearer pattern.

IV. Discussion

A. Summary of current results and previous work

We have now investigated the dissociation dynamics of HOCl with different amounts of vibrational energy deposited selectively into the OH stretch coordinate. As explained above, the dynamics in these three energy regions exhibit remarkably different features:

At (6,0,0), which is just above the dissociation threshold, we observe extremely slow dissociation rates (2×10^6–3×10^8 s^{-1}) and large state-to-state variation with rotational quantum number. Weak vibrational coupling is apparent from the spectra.

At (7,0,0), which is ~ 2400 cm^{-1} above the threshold, we measure dissociation rates in the range 1–4×10^9 s^{-1}. No prominent rate variation is apparent over the small number of rotational states investigated, and there is no evidence of vibrational coupling from the appearance of additional spectral features, although the large distortion constant suggests uniform non-resonant coupling across the entire band.

At (8,0,0), which is ~ 4800 cm^{-1} above threshold, the dissociation rates are fast and exhibit clear patterns with increasing J over the range of rotational states investigated. Strong vibrational coupling is apparent from spectral splittings and from perturbations in the expected line positions.

As a starting point for interpreting the dynamics after excitation to (7,0,0) and (8,0,0), we use the physical model introduced in our previous work for (6,0,0). There, the
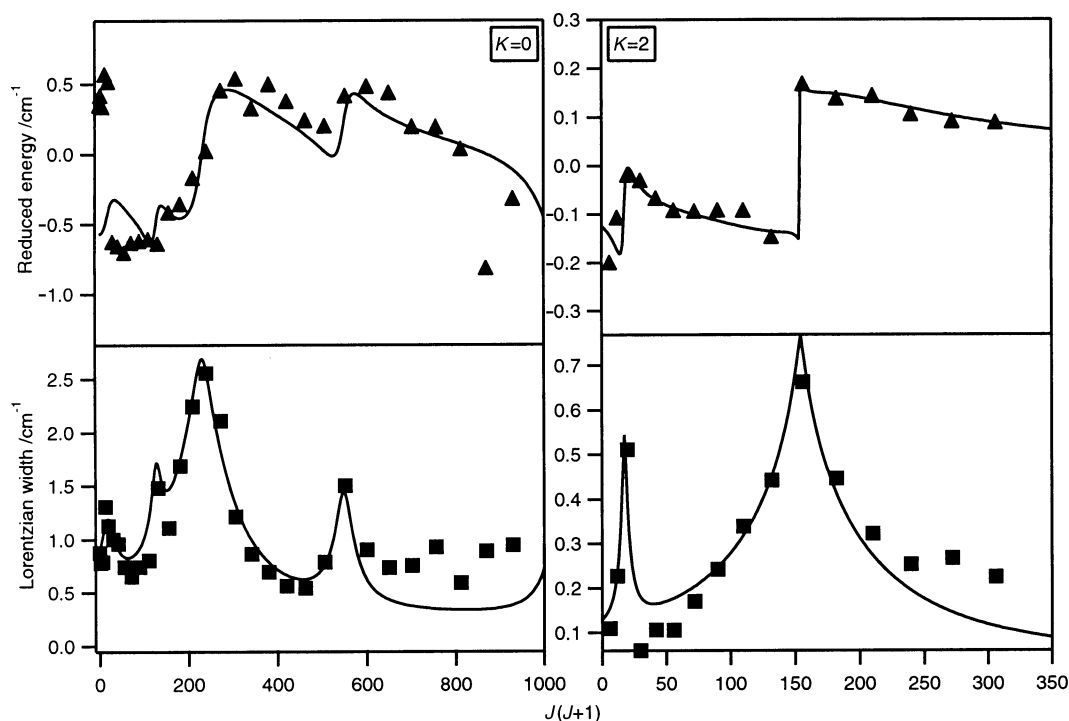
Fig. 4 Observed rotational dependence of energy (top panels) and width (bottom panels) of HOCl $v_{\mathrm{OH}} = 8$ states. In order to better show the effect of perturbations, the energy of a rigid rotor with the constants of Table 1 has been subtracted from the total energy and the resulting reduced energy plotted. Hence, if no perturbation were present, all rotational states would have zero reduced energy, within the experimental uncertainty. The effect of interaction with perturbing states (solid line) has been modeled with the Hamiltonian in eqn. (5) and the following parameters (in cm^{-1}): at $K = 0$, $\Gamma_0^0 = 0.25$; $\Gamma_i^0 = 10$; $W_{0i} = 1.2, 1.2, 2, 1.5, 3$; $B_i - B_0 = -0.2, -0.3, -0.05, -0.15, -0.25$; at $K = 2$, $\Gamma_0^0 = 0.04$; $\Gamma_i^0 = 2, 1.5$; $W_{0i} = 0.4, 0.4$; $B_i - B_0 = -0.2, -0.01$.

spectroscopic evidence, together with calculated wavefunctions[47] using *ab initio* potential energy surfaces, indicates that the initially prepared states largely preserve their zeroth-order character. In the zeroth-order approximation where the three vibrational modes are separable along the OH stretching, HOCl bending and OCl stretching coordinates, the pure OH stretching levels do not dissociate—it is only through vibrational mixing with states that have sufficient energy in the dissociation coordinate that they acquire a finite lifetime. Thus, the long lifetime of (6,0,0), as well as the sharp state-to-state fluctuations observed, arise from weak, non-uniform mixing with rapidly dissociating states.

B. Vibrational character of (7,0,0) and (8,0,0)

Before interpreting the dynamics of the (7,0,0) and (8,0,0) levels, one must ask if the zeroth-order description of the initially prepared state is still appropriate at these high energies? The answer is clear for (7,0,0), where the fit of line positions and the lack of additional spectral features suggest that the initially prepared state maintains most of its original OH stretch character. For the (8,0,0) level, the appearance of many perturbing states in the spectra indicates that assumption of a pure OH stretch begins to break down. We can get information on the degree of this breakdown from the analysis of the vibrational dependence of the molecular constants. The energies of the $(v,0,0)$ OH stretch band origins are expected to follow the formula

$$\nu_0(v) = av + bv^2 \qquad (3)$$

as long as the potential along this coordinate is well approximated by a Morse function. As shown in Fig. 5 top panel, a Birge–Sponer plot of ν_0/v *vs.* v gives an excellent fit to the data, indicating that the Morse approximation holds well as high as $v_{OH} = 8$. While linearity of the Birge–Sponer plot in itself is not evidence for a localized OH stretch, the similarity of the parameters to those obtained for other OH containing molecules[18,65–67] and for the OH radical itself[68] indicates that the OH stretch behaves like a local mode. Similar information is obtained from the vibrational dependence of the rotational constants. Since HOCl is almost a symmetric top, with the a-axis nearly coincident with the O–Cl bond, the value of $A - B$ is mostly determined by the OH bond length and the HOCl bending angle. Anomalous changes of this constant would signal a change in the nature of the initially prepared state. The nearly linear progression of $A - B$ displayed in Fig. 5, bottom panel, is an indication that the initially prepared state maintains a substantial fraction of its zeroth-order OH stretch character, even at $v_{OH} = 8$.

C. Vibrational state dependence of IVR and unimolecular dissociation dynamics

1. Increasing average dissociation rate. Having established that the (7,0,0) and (8,0,0) levels largely retain their zeroth-order OH stretch character, we now discuss the evolution of the observed rates shown in Fig. 6 as a function of the OH stretch quantum number. Two features become immediately evident with increasing v_{OH}: the average of the rates that we measure increases by two orders of magnitude per OH quantum and the distribution of rates narrows. Given our earlier conclusion that dissociation rates at (6,0,0) are limited by IVR, the increase of the average dissociation rate implies a corresponding increase in the IVR rate. Qualitatively, this is not surprising, since the IVR rate is proportional to the density of states and the mean square coupling, both of which are expected to increase with energy. Since the density of states does not increase dramatically[55] (about a factor of 2 per each additional quanta of OH stretching vibration), most of
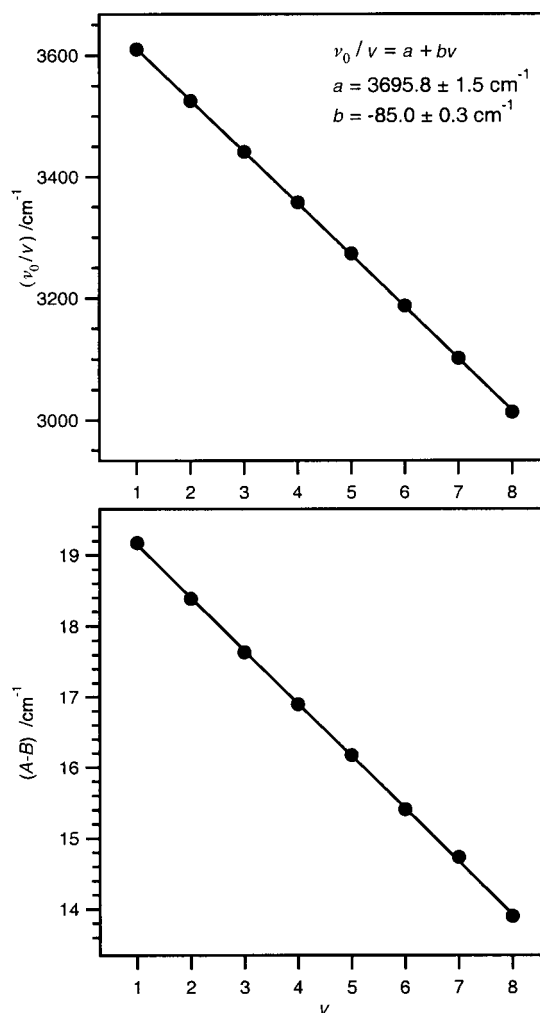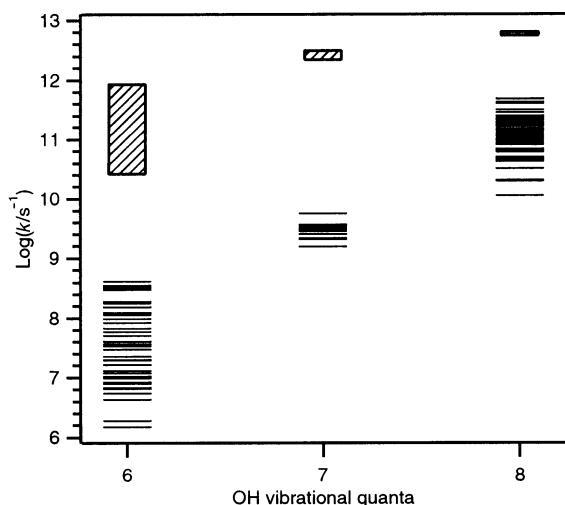

Fig. 5 Vibrational dependence of HOCl molecular constants. Top panel: Birge–Sponer plot. Bottom panel: $A - B$.

the difference is likely due to increased coupling strength. Using Fermi's golden rule

$$\Gamma_{IVR} = 2\pi w^2 \rho \qquad (4)$$

with a density of states[55] $\rho = 0.36$ states per cm^{-1} yields coupling matrix elements $w \sim 0.08$–0.12 cm^{-1} for (7,0,0). Given the small magnitude of the coupling compared to average level spacing, together with the relatively small range of rotational levels investigated, it is not surprising that no perturbations are visible in the measured energy of rotational levels. Using a density of states[55] of 0.6 per cm^{-1} for the energy region of (8,0,0), the same expression gives w in the range 0.23–0.8 cm^{-1}, with a rms value of 0.45 cm^{-1}, only slightly smaller than the average level spacing. Given the non-uniform nature of the vibrational state distribution, this finding agrees well with our observation of spectral perturbations in this energy region.

While our estimates for the average coupling matrix elements are consistent with our spectral observations, it is not clear why these couplings, and hence the dissociation rates, should increase so sharply with v_{OH}. Scaling of the coupling matrix elements with the number of vibrational quanta certainly plays a role, but this is not nearly sufficient to account for the 5-fold average increase between (7,0,0) and (8,0,0), particularly if only low-order couplings are considered. We can gain some insight into this question by looking at the HOCl potential energy surface (Fig. 4 of ref. 41 and Fig. 1 of ref. 54). In particular, by examining the surface in the R_{OH}–θ plane one can deduce the degree of interaction between the OH stretch-

Fig. 6 Vibrational dependence of HOCl unimolecular decay rate distribution and comparison with RRKM calculations. Each thin horizontal line corresponds to the observed rate of an individual J,K rotational state, while the boxes indicate the distribution expected under the assumption of validity of RRKM theory (complete state mixing). At $v_{OH} = 6$, only rotational states for which a single product channel is energetically accessible have been included in the experimental distribution. The theoretical distribution is a χ^2 distribution with as many degrees of freedom as the number of open channels (1, 11 and 24, respectively at $v_{OH} = 6$, 7 and 8) and average given by the RRKM theory. For the number of open channels a lower estimate has been used, counting one channel per each rotational state of the OH fragment energetically accessible, without including the different spin–orbit states of the fragments. Note that a more realistic estimate would further increase the discrepancy between the observed and calculated distributions.

ing and HOCl bending motion. While the surface is regular at low energy, at energies above 55 kcal mol^{-1}, significant distortion is apparent in the range $R_{OH} = 2.3$–3 a_0 and $\theta = 50$–70° where the pathway to the HClO isomer is located. The energies of the $v_{OH} = 6$, 7 and 8 levels are, for this two-dimensional oscillator, about 61.6, 69.0 and 75.8 kcal mol^{-1} respectively, above the potential minimum, so one can expect that the distorted region plays an increasingly important role in the stretch–bend energy redistribution.

It is important to note that despite the strong increase in dissociation rate with increasing v_{OH} displayed in Fig. 6, the average rate is still 1–2 orders of magnitude slower than the predictions of statistical theories.

2. Narrower rate fluctuations at higher energies. The second important feature of the observed distribution of dissociation rates (Fig. 6) is a narrowing spread about the average value with increasing v_{OH}. While for (7,0,0) this is, at least in part, due to the small sample of rotational states investigated, the same argument does not hold for (8,0,0). In paper II we had reasoned that the dissociation rate of each rovibrational state is determined by the extent of its mixing with fast-dissociating bath states. In turn, the relative position of these states, and hence the extent of this mixing, changes with J and K since they have slightly different rotational constants. In the case of (6,0,0), the weak coupling, low density of bath states and narrow widths would imply that the actual rate is determined primarily by interaction with a single bath state at a time. Hence, a sharp increase in the rate is observed whenever the bright state is "accidentally' in resonance with a bath state. We propose a similar mechanism to explain our results at (7,0,0) and (8,0,0), taking into account certain important differences expected in these higher energy regions. At higher values of v_{OH}, the stronger coupling of the bright state to the bath states, together with a slightly higher state density and

an increased average width (determined by the dissociation rate) suggest that the bright state dissociation rate will be controlled by mixing with several bath states at a time. Moreover, the distribution of unimolecular dissociation rates is expected to narrow at higher energies above dissociation threshold as more independent product channels become available.[8,64] In the light of these differences from the (6.0.0) region, we suggest that the rate fluctuations from one rotational state to the next still arise from differences in the slight degree of mixing between the bright state and bath states, but that the various coupling pathways are more equivalent to one another, partially washing out the sharp rate fluctuations.

3. Correlation between unimolecular dissociation rates and spectral perturbations. Fig. 4 clearly reinforces this interpretation for the rate fluctuations that we observe at (8,0,0) by demonstrating their direct correspondence with the spectral perturbations that reflect vibrational coupling. Our treatment of these fluctuations is analogous to that used to explain the dynamics at (6,0,0), however in the present case we must consider several perturbers simultaneously. We use for this purpose a Hamiltonian of the form

$$\mathbf{H} = \begin{pmatrix} E_0^0 - i\dfrac{\Gamma_0^0}{2} & W_{01} & \cdots & W_{0n} \\ W_{01} & E_1^0 - i\dfrac{\Gamma_1^0}{2} & & \mathbf{0} \\ \vdots & & \ddots & \\ W_{0n} & \mathbf{0} & & E_n^0 - i\dfrac{\Gamma_n^0}{2} \end{pmatrix} \quad (5)$$

In this model, the bright state (identified by the subscript $i = 0$) and the bath states (identified by the subscript $i = 1\cdots n$) have zeroth order energies E_i^0 and decay widths Γ_i^0. Only coupling between the bright state and the bath states (W_{0i}) is considered. The energies are J-dependent through $E_i^0 = E_i^0|_{J=0} + B_i J(J + 1)$, i.e. the relative position of the states changes with J.

Using the above Hamiltonian we can satisfactorily establish a correspondence, albeit only qualitative, between the tuning-in resonance of dark perturbing states and the peaks in the dissociation rate observed at $K = 0$ and $K = 2$, as shown in Fig. 4. The inability of this model to reproduce quantitatively the experimental observations comes from the fact that it does not allow for interaction between the bath states, which we believe to play an important role at these energies. Unfortunately, the number of adjustable parameters grows rapidly with the number of states in a fully coupled model, thus making it unmanageable for our purposes. On the other hand, having been able to reproduce the main features of the experimental data with such a simple model shows that even at the high energies involved here, the vibrational dynamics that mediates the dissociation still preserves a large degree of regularity, in spite of the rapid increase of the couplings with the number of v_{OH} quanta.

V. Summary and conclusions

We have investigated the spectroscopy and unimolecular reaction dynamics of HOCl prepared in single rotational states with 7 and 8 quanta of OH stretching vibration. Together with our previous work at (6,0,0), these results give us a broader view of the interplay between intramolecular vibrational energy redistribution and unimolecular dissociation. The dissociation rates at (6,0,0), which are 4–6 orders of magnitude slower than predicted by statistical theories, appear to be dominated by the slow IVR rate. As we deposit 7 or 8 quanta into the OH stretch, we observe a rapid increase in the

dissociation rate that approaches the statistical limit without reaching it at (8,0,0). Consistent with the increased IVR rate at the higher energies, we observe numerous, strong perturbations at of the (8,0,0) level, indicating substantial mixing between the zeroth-order vibrational modes.

The fact that HOCl dissociation dynamics is not well described by a statistical model, even at energies as high as 5000 cm^{-1} above the dissociation threshold, has important consequences for unimolecular reaction theories that are based on this assumption, most notably, the fact that a microcanonical ensemble of molecules would not decay exponentially as predicted by such theories.

References

1   O. K. Rice and H. C. Ramsperger, *J. Am. Chem. Soc.*, 1927, **49**, 1617.
2   O. K. Rice and H. C. Ramsperger, *J. Am. Chem. Soc.*, 1928, **50**, 617.
3   L. S. Kassel, *J. Phys. Chem.*, 1928, **32**, 225.
4   P. J. Robinson and K. A. Holbrook, *Unimolecular Reactions*, Wiley, New York, 1972.
5   M. Quack and J. Troe, *Ber. Bunsen-Ges. Phys. Chem.*, 1974, **78**, 240.
6   W. F. Polik, D. R. Guyer and C. B. Moore, *Proc. SPIE—Int. Soc. Opt. Eng.*, 1988, **912**, 150.
7   W. F. Polik, C. B. Moore and W. H. Miller, *J. Chem. Phys.*, 1988, **89**, 3584.
8   W. F. Polik, D. R. Guyer, W. H. Miller and C. B. Moore, *J. Chem. Phys.*, 1990, **92**, 3471.
9   W. F. Polik, D. R. Guyer and C. B. Moore, *J. Chem. Phys.*, 1990, **92**, 3453.
10 J. D. Tobiason, J. R. Dunlop and E. A. Rohlfing, *J. Chem. Phys.*, 1995, **103**, 1448.
11 J. D. Tobiason, J. R. Dunlop and E. A. Rohlfing, *Chem. Phys. Lett.*, 1995, **235**, 3.
12 D. W. Neyer, L. Xin, I. Burak and P. L. Houston, *J. Chem. Phys.*, 1995, **102**, 1645.
13 G. W. Adamson, X. Zhao and R. W. Field, *J. Mol. Spectrosc.*, 1993, **160**, 11.
14 Y. S. Choi and C. B. Moore, *J. Chem. Phys.*, 1989, **90**, 3875.
15 A. Geers, J. Kappert, F. Temps and J. W. Wiebrecht, *J. Chem. Phys.*, 1993, **99**, 2271.
16 A. Mellinger, M. V. Ashikhmin and C. B. Moore, *J. Chem. Phys.*, 1998, **108**, 8944.
17 B. R. Foy, M. P. Casassa, J. C. Stephenson and D. S. King, *J. Chem. Phys.*, 1990, **92**, 2782.
18 B. Kuhn and T. R. Rizzo, *J. Chem. Phys.*, 2000, **112**, 7461.
19 M. R. Wedlock, R. Jost and T. R. Rizzo, *J. Chem. Phys.*, 1997, **107**, 10344.
20 A. Callegari, J. Rebstein, J. S. Muenter, R. Jost and T. R. Rizzo, *J. Chem. Phys.*, 1999, **111**, 123.
21 A. Callegari, J. Rebstein, R. Jost and T. R. Rizzo, *J. Chem. Phys.*, 1999, **111**, 7359.
22 R. J. Barnes, G. Dutton and A. Sinha, *J. Phys. Chem. A*, 1997, **101**, 8374.
23 R. J. Barnes and A. Sinha, *J. Chem. Phys.*, 1997, **107**, 3730.
24 G. Dutton, R. J. Barnes and A. Sinha, *J. Chem. Phys.*, 1999, **111**, 4976.
25 J. S. Wells, R. L. Sams and W. J. Lafferty, *J. Mol. Spectrosc.*, 1979, **77**, 349.
26 R. L. Sams and W. B. Olson, *J. Mol. Spectrosc.*, 1980, **84**, 113.
27 M. Carlotti, G. Di Lonardo, L. Fusina, A. Trombetti and B. Carli, *J. Mol. Spectrosc.*, 1990, **141**, 29.
28 F. Cavazza, G. Di Lonardo, R. Escribano, L. Fusina, P. C. Gomez and J. Ortigoso, *J. Mol. Spectrosc.*, 1993, **159**, 395.
29 C. Azzolini, F. Cavazza, G. Crovetti, G. Di Lonardo, R. Frulla, R. Escribano and L. Fusina, *J. Mol. Spectrosc.*, 1994, **168**, 494.
30 M. L. Juntilla, W. J. Lafferty and J. B. Burkholder, *J. Mol. Spectrosc.*, 1994, **164**, 583.
31 B. Abel, H. H. Hamann, A. A. Kachanov and J. Troe, *J. Chem. Phys.*, 1996, **104**, 3189.
32 F. Cavazza, G. Di Lonardo and L. Fusina, *Gazz. Chim. Ital.*, 1996, **126**, 539.
33 R. M. Escribano, G. Di Lonardo and L. Fusina, *Chem. Phys. Lett.*, 1996, **259**, 5.
34 B. Abel, A. Charvat, S. F. Deppe and H. H. Hamann, *Ber. Bunsen-Ges. Phys. Chem.*, 1997, **101**, 329.
35 A. Charvat, S. F. Deppe, H. H. Hamann and B. Abel, *J. Mol. Spectrosc.*, 1997, **185**, 336.
36 H. H. Hamann, A. Charvat, B. Abel, S. A. Kovalenko and A. A. Kachanov, *J. Chem. Phys.*, 1997, **106**, 3103.
37 K. A. Peterson, *Spectrochim. Acta, Part A*, 1997, 1051.
38 J. M. Flaud, M. Birk, G. Wagner, J. Orphal, S. Klee and W. J. Lafferty, *J. Mol. Spectrosc.*, 1998, **191**, 362.
39 J. Koput and K. A. Peterson, *Chem. Phys. Lett.*, 1998, **283**, 3.
40 S. Skokov, J. X. Qi, J. M. Bowman, C. Y. Yang, S. K. Gray, K. A. Peterson and V. A. Mandelshtam, *J. Chem. Phys.*, 1998, **109**, 10273.
41 S. Skokov, K. A. Peterson and J. M. Bowman, *J. Chem. Phys.*, 1998, **109**, 2662.
42 J. Hauschildt, J. Weiss, C. Beck, S. Grebenshchikov, R. Duren, R. Schinke and J. Koput, *Chem. Phys. Lett.*, 1999, **300**, 5.
43 R. Jost, M. Joyeux, S. Skokov and J. Bowman, *J. Chem. Phys.*, 1999, **111**, 6807.
44 K. A. Peterson, S. Skokov and J. M. Bowman, *J. Chem. Phys.*, 1999, **111**, 7446.
45 C. Rongqing, G. Hua, S. Skokov and J. M. Bowman, *J. Chem. Phys.*, 1999, **111**, 7290.
46 S. Skokov, J. M. Bowman and V. A. Mandelshtam, *Phys. Chem. Chem. Phys.*, 1999, **1**, 1279.
47 S. Skokov and J. M. Bowman, *J. Chem. Phys.*, 1999, **110**, 9789.
48 S. Skokov, K. A. Peterson and J. M. Bowman, *Chem. Phys. Lett.*, 1999, **312**, 5.
49 S. Skokov and J. M. Bowman, *J. Chem. Phys.*, 1999, **111**, 4933.
50 H. Zhang, B. Ramachandran, J. Senekowitsch and R. E. Wyatt, *THEOCHEM*, 1999, **487**, 1.
51 J. Hauschildt, J. Weiss and R. Schinke, *Z. Phys. Chem.*, 2000, **5**, 609.
52 M. Joyeux, D. Sugny, M. Lombardi, R. Jost, R. Schinke, S. Skokov and J. Bowman, *J. Chem. Phys.*, 2000, **113**, 9610.
53 J. Vander Auwera, J. Kleffmann, J. M. Flaud, G. Pawelke, H. Burger, D. Hurtmans, R. Petrisse, B. R. Foy, M. P. Casassa, J. C. Stephenson and D. S. King, *J. Mol. Spectrosc.*, 2000, **204**, 36.
54 J. Weiss, J. Hauschildt, S. Y. Grebenshchikov, R. Duren, R. Schinke, J. Koput, S. Stamatiadis and S. C. Farantos, *J. Chem. Phys.*, 2000, **112**, 77.
55 S. Zou, S. Skokov and J. M. Bowman, *Chem. Phys. Lett.*, 2001, in press.
56 L. Halonen and T. K. Ha, *J. Chem. Phys.*, 1988, **88**, 3775.
57 C. H. Townes and A. L. Schawlow, *Microwave spectroscopy*, Dover Publications, New York, 1975.
58 D. Papousek and M. R. Aliev, *Molecular Vibrational–rotational Spectra: Theory and Applications of High Resolution Infrared, Microwave and Raman Spectroscopy of Polyatomic Molecules*, Elsevier, Amsterdam, 1982.
59 J. R. Fair, O. Votava and D. J. Nesbitt, *J. Chem. Phys.*, 1998, **108**, 72.
60 O. V. Boyarkin, T. R. Rizzo and D. S. Perry, *J. Chem. Phys.*, 1999, **110**, 11346.
61 J. Humlicek, *J. Quant. Spectrosc. Radiat. Transfer*, 1982, **27**, 437.
62 F. Schreier, *J. Quant. Spectrosc. Radiat. Transfer*, 1992, **48**, 743.
63 R. Schinke and J. Weiss, personal communication.
64 W. H. Miller, R. Hernandez, C. B. Moore and W. F. Polik, *J. Chem. Phys.*, 1990, **93**, 5657.
65 J. L. Scott, D. Luckhaus, S. S. Brown and F. F. Crim, *J. Chem. Phys.*, 1995, **102**, 675.
66 O. V. Boyarkin, L. Lubich, R. D. F. Settle, D. S. Perry and T. R. Rizzo, *J. Chem. Phys.*, 1997, **107**, 8409.
67 F. Reiche, B. Abel, R. D. Beck and T. R. Rizzo, *J. Chem. Phys.*, 2000, **112**, 8885.
68 J. A. Coxon and S. C. Foster, *Can. J. Phys.*, 1982, **60**, 41.